Quantum-state-selective decay spectroscopy of ^{213}Ra

Ch. Lorenz,[1] L. G. Sarmiento,[1,2] D. Rudolph,[1] D. E. Ward,[1] M. Block,[3,4,5] F. P. Heßberger,[3,4] D. Ackermann,[3] L.-L. Andersson,[4,6] M. L. Cortés,[2,3,7] C. Droese,[8] M. Dworschak,[3] M. Eibach,[8,9,10] U. Forsberg,[1] P. Golubev,[1] R. Hoischen,[1,3] I. Kojouharov,[3] J. Khuyagbaatar,[3,4] D. Nesterenko,[3,11] I. Ragnarsson,[1] H. Schaffner,[3] L. Schweikhard,[8] S. Stolze,[3,12] and J. Wenzl[10]

[1]*Department of Physics, Lund University, S-22100 Lund, Sweden*
[2]*Departamento de Física, Universidad Nacional de Colombia, CO-111321 Bogotá D.C., Colombia*
[3]*GSI Helmholtzzentrum für Schwerionenforschung, D-64291 Darmstadt, Germany*
[4]*Helmholtz-Institut Mainz, D-55099 Mainz, Germany*
[5]*Institut für Kernchemie, Johannes Gutenberg-Universität, D-55128 Mainz, Germany*
[6]*Department of Physics, University of Liverpool, L69 7ZE Liverpool, United Kingdom*
[7]*RIKEN Nishina Center, 2-1 Hirosawa, Wako, 351-0198 Saitama, Japan*
[8]*Institut für Physik, Ernst-Moritz-Arndt-Universität, D-17487 Greifswald, Germany*
[9]*Institut für Physik, Johannes Gutenberg-Universität, D-55128 Mainz, Germany*
[10]*National Superconducting Cyclotron Laboratory, East Lansing, 48824 Michigan, USA*
[11]*Petersburg Nuclear Physics Institute, St. Petersburg, 188300 Leningradskaya oblast, Russia*
[12]*Department of Physics, University of Jyväskylä, FI-40014 Jyväskylä, Finland*

(Received 19 June 2017; published 18 September 2017)

An experimental scheme combining the mass resolving power of a Penning trap with contemporary decay spectroscopy has been established at GSI Darmstadt. The Universal Linear Accelerator (UNILAC) at GSI Darmstadt provided a ^{48}Ca beam impinging on a thin ^{170}Er target foil. Subsequent to velocity filtering of reaction products in the Separator for Heavy Ion reaction Products (SHIP), the nuclear ground state of the 5*n* evaporation channel ^{213}Ra was mass-selected in SHIPTRAP, and the ^{213}Ra ions were finally transferred into an array of silicon strip detectors surrounded by large composite germanium detectors. Based on comprehensive GEANT4 simulations and supported by theoretical calculations, the spectroscopic results call for a revision of the decay path of ^{213}Ra, thereby exemplifying the potential of a combination of a mass-selective Penning trap device with a dedicated nuclear decay station and contemporary GEANT4 simulations.

DOI: 10.1103/PhysRevC.96.034315

I. INTRODUCTION

Contemporary nuclear structure studies aim at investigations of nuclei far from the line of β stability. While the neutron-rich outskirts of the nuclidic chart can preferentially be reached by fragmentation or fission of relativistic heavy-ion beams, fusion-evaporation reactions continue to compete on the neutron-deficient side and remain the exclusive way to produce very heavy or superheavy elements (SHE).

With production cross sections in the regime of μb down to pb, however, the task of preparing isotopically clean sources and, thus, unambiguous decay information becomes ever more essential and challenging: Even in the focal planes of velocity and/or A/q recoil separators, proverbially, the nuclidic needles of interest can be hidden in a hay stack of either isobars in the case of neutron-deficient nuclei or the inevitable background of mostly target-like transfer reaction products in the case of SHE studies.

A rather new approach to such kind of isotope-selective spectroscopy is the possibility to first select a well defined nuclear quantum state by means of a precision mass selection in a Penning trap. Subsequently, the nuclei in that particular quantum state can be transferred into a given decay spectroscopy station.

A first experiment employing trap-assisted spectroscopy was performed with REXTRAP at ISOLDE/CERN for conversion electron studies [1]. More recently, the JYFLTRAP system at the University of Jyväskylä was employed in conjunction with a movable-tape station for selective $\beta\gamma(\gamma)$-decay studies of neutron-rich Zr, Ru, and Tc isotopes [2–4]. In the meantime similar schemes were successfully employed at ISOLDE/CERN with decay stations positioned either behind ISOLTRAP's precision Penning trap [5,6] or its multireflection time-of-flight component [7].

In the present case, the TASISpec detector system [8] has been placed directly behind SHIPTRAP at GSI Darmstadt, Germany [9]. Coincidences between α particles and γ rays as well as x rays have been detected and α-β^+/electron-capture (EC) branching ratios following the decay of the ground state of ^{213}Ra have been investigated.

Comprising $N = 125$ neutrons, decay properties of ^{213}Ra and both its α- and β^+/EC-decay daughters carry primarily information on the shell structure of neutron-deficient nuclei in the vicinity of the magic neutron number $N = 126$. The first experimental studies of ^{213}Ra date back to the 1960s [10,11], when He-jet techniques were applied to study the decay of neutron-deficient radium isotopes. In fact, both the proposed α-β^+/EC branching ratio as well as the leading α-decay branching ratios into the ground, first excited, and second excited states of ^{209}Rn remained unchanged since then [12,13]. The situation is similar for the main decay characteristics of

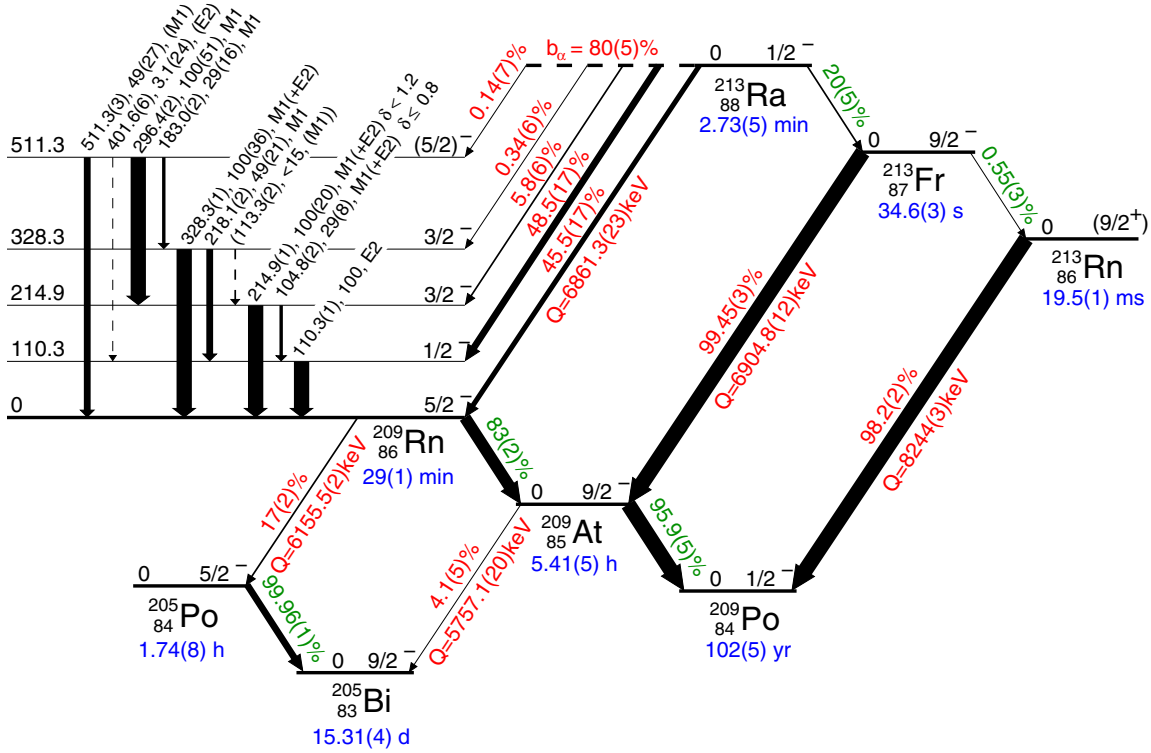

FIG. 1. Adopted decay scheme of the ^{213}Ra ground-state decay path based on the evaluated data in Refs. [13,18,22]. α-decay branching ratios and Q values are presented in red, β^+/EC-decay branching ratios in green.

Fr, Rn, or At daughter nuclei [14–17], here produced as α- or β^+/EC-decay daughters of ^{213}Ra. The evaluated half-life of the ground state of ^{213}Ra is $T_{1/2} = 2.73(5)$ minutes [18].

While confirming these early results, still based on He-jet techniques, Raich *et al.* [19] performed the first α-γ coincidence study of ^{213}Ra, thereby also establishing a 2.15 ms, $17/2^-$ isomeric state at 1770 keV. ^{213m}Ra has been confirmed in a more recent systematic study of high-spin isomers in a chain of radium isotopes by Heßberger *et al.* [20], using a recoil separator in conjunction with recoil-decay correlation techniques.

The hitherto most comprehensive experimental study of the decay of both ^{213}Ra and ^{213m}Ra was put forward by Kuusiniemi *et al.* [21]. With the results being consistent with previous observations, an additional α-decay branch with a relative yield below 1% was proposed, discussed in a systematic fashion together with a series of $N = 125$ isotones. Nevertheless one should note that the results obtained in Ref. [21] rely on the α-β^+/EC branching ratios and the α-decay branching ratios into the ground and first excited states of ^{209}Rn from the first experimental studies of ^{213}Ra.

Figure 1 comprises evaluated data relevant for this work. In Table I all the transitions in ^{209}Rn are listed, including conversion coefficients and transition branching-ratios.

In the present study, following a description of the experiment, the results are confronted with extensive GEANT4 simulations. The derived results are then compared to theoretical predictions, in particular the relative α-decay branching ratios.

A brief description of the experimental procedure and preliminary results are provided in Ref. [24].

II. EXPERIMENT

The experiment was performed at the GSI Helmholtz Centre for Heavy Ion Research in Darmstadt, Germany. The

TABLE I. Evaluated level energies E_x, γ-ray energies E_γ and relative intensities I_γ, conversion coefficients $\alpha_{\rm tot}$ [23], transition branching ratios b_t, multipolarity $T\lambda$, and spin-parity assignments of observed states in ^{209}Rn [13].

E_x (keV)	E_γ (keV)	I_γ (%)	$\alpha_{\rm tot}$ [23]	b_t (%)	$T\lambda$	$I_i^\pi \rightarrow I_f^\pi$
110.3(1)	110.3(1)	100	5.48(8)	100	$E2$	$\frac{1}{2}^- \rightarrow \frac{5}{2}^-$
214.9(1)	214.9(1)	100(20)	1.50(3)	41(5)	$M1$[a]	$\frac{3}{2}^- \rightarrow \frac{5}{2}^-$
	104.8(2)	29(8)	11.4(2)	59(5)	$M1$[a]	$\frac{3}{2}^- \rightarrow \frac{1}{2}^-$
328.3(1)	328.3(1)	100(36)	0.467(7)	56(10)[b]	$M1$[a]	$\frac{3}{2}^- \rightarrow \frac{5}{2}^-$
	218.1(2)	49(21)	1.44(2)	44(10)[b]	$M1$[a]	$\frac{3}{2}^- \rightarrow \frac{1}{2}^-$
	113.3(2)	<15	9.2(2)		$M1$[a]	$\frac{3}{2}^- \rightarrow \frac{3}{2}^-$
511.3(2)	511.3(3)	49(27)	0.141(2)	17(5)	$M1$[c]	$(\frac{5}{2})^- \rightarrow \frac{5}{2}^-$
	401.6(6)	3.1(24)	0.0608(9)	1.0(7)	$E2$[c]	$(\frac{5}{2})^- \rightarrow \frac{1}{2}^-$
	296.4(2)	100(51)	0.617(9)	51(12)	$M1$[c]	$(\frac{5}{2})^- \rightarrow \frac{3}{2}^-$
	183.0(2)	29(16)	2.36(9)	31(11)	$M1$[c]	$(\frac{5}{2})^- \rightarrow \frac{3}{2}^-$

[a]Assuming pure transition. However, admixtures of $E2$ are not excluded [21].
[b]Excluding the proposed 113.3 keV transition.
[c]The multipolarity of those transitions and the spin-parity of the 511 keV state have not been measured yet and are only assumed.

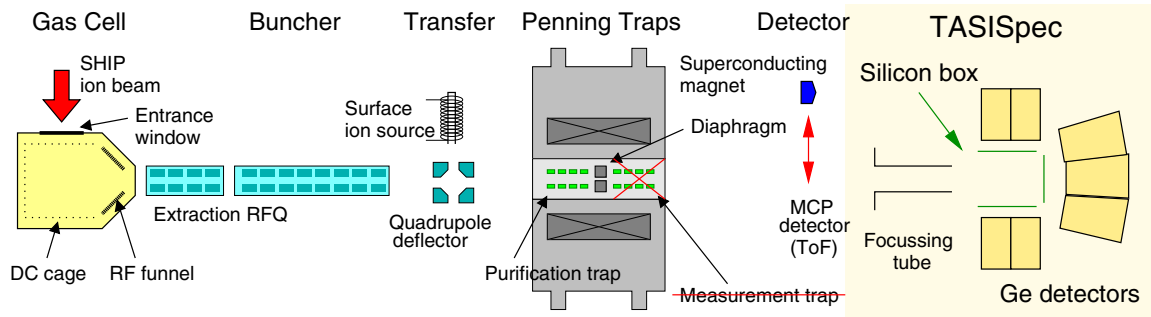

FIG. 2. Sketch of the "TRAPSpec" experimental setup starting with the stopping gas cell of SHIPTRAP located behind the focal plane of the velocity filter SHIP [25]. $^{213}Ra^{2+}$ ions are chosen and transferred into the first of the two traps (purification trap). Following the selection of the mass of the ground state of ^{213}Ra, the residues are sent into the TASISpec decay station [8]. The second trap (measurement trap) was not employed in this experiment. See text for details.

Universal Linear Accelerator (UNILAC) facility provided a ^{48}Ca beam at an energy of 4.30 MeV/u and an average beam intensity of about 0.1 particle-μA. The ^{48}Ca ions impinged on a rotating target wheel comprising ten segments of $\sim$0.4 mg/cm^2 thick, isotopically enriched ^{170}Er layers evaporated onto $\sim$30 μg/cm^2 thin ^{12}C backings. The residues of the fusion-evaporation reaction, among others, ^{170}Er(^{48}Ca,5n)^{213}Ra, were separated from primary beam particles and nuclear transfer products by the velocity filter SHIP [25]. The transmission of residual nuclei towards the focal plane of SHIP was verified and controlled with a movable silicon detector, recording the implantation and identifying subsequent α decays of heavy ions.

For the major part of the experiment, this silicon detector was removed. Instead, the ions entered the stopping gas cell at the entrance of SHIPTRAP [26], which is shown on the left-hand side of Fig. 2. The next step involved optimizing the purification of ^{213}Ra ions. For ^{213}Ra, singly and doubly charged ions were extracted from the gas cell within a few milliseconds. In the present case a higher yield of $^{213}Ra^{2+}$ ions in comparison to $^{213}Ra^{+}$ ions was obtained. Thus, all further preparation steps were carried out on $^{213}Ra^{2+}$ ions. They were cooled and accumulated in the radio-frequency quadrupole buncher before they were transferred to the purification (Penning) trap in short bunches. Ions were accumulated in the buncher in parallel to the preparation of the ion samples in the trap. In the purification trap, a mass-selective buffer gas cooling technique was employed [27]. The mass resolving power reached $m/\delta m = 72\,000$, corresponding to $\sim$2.7 MeV, during the experiment for a cycle time of $\sim$400 ms. Since the half-life of the 2.15 ms isomeric state ^{213m}Ra at 1770 keV is orders of magnitudes shorter than the cycle time, it has decayed before the beam is delivered to the decay station. ^{213}Fr, of which the ground state is only $\sim$3.9 MeV below the ^{213}Ra ground state, has a second ionization potential close to the first one of helium, which is used in the stopping gas cell. Therefore, $^{213}Fr^{2+}$ ions recombine there and were not extracted from the gas cell. This scheme allowed for a preparation of a pure beam of ^{213}Ra ions in their nuclear ground state. Hence it was not necessary to employ the high-resolution measurement trap for the decay spectroscopy part of the experiment.

However, for an unambiguous identification a mass measurement of ^{213}Ra was performed in the second trap, the so-called measurement trap, of SHIPTRAP [9]. To this end, the cyclotron frequency of $^{213}Ra^{2+}$ was compared to the cyclotron frequency of $^{133}Cs^{+}$, a calibrant ion produced in a surface ion source [28].

On average, 2–3 $^{213}Ra^{2+}$ ions per second were extracted from the purification trap. This rate was measured with the standard microchannel plate (MCP) detector located at the exit of SHIPTRAP, which has a detection efficiency of about 35%.

Finally, the MCP detector at the exit of SHIPTRAP was removed from the beam axis, and the ^{213}Ra nuclei were allowed to enter the TASISpec decay station [8] through a focusing tube. In conjunction with the acceleration, deflection, and focusing elements of SHIPTRAP, an optimum near 100% transmission was achieved with a voltage of $U_{\text{tube}} = -300$ V and on average about 30% reduced bias high-voltages on the four single-sided silicon strip detectors (SSSSD). These formed the upstream part of the TASISpec silicon box. Interestingly, the negative bias voltages of these 1.0 mm thick detectors can noticeably deflect the rather slow radium ions [24] away from the beam axis, because the kinetic energy of the ions is as low as few keV. The reduced bias voltage does not alter the performance of the TASISpec box detectors significantly, in particular not for α-decay spectroscopy since their "p" sides face the inner part of the silicon box, while the depletion zone grows with increasing bias towards their "n" sides.

In addition to the four sides of the box (the signals of one unfortunately could not be processed), the silicon box was complemented by one double-sided silicon strip detector (DSSSD) located downstream with an intrinsic resolution of 20–25 keV FWHM and a dead layer of $\approx$2 μm [29,30]. This detector was 0.31 mm thick and provided $32 \times 32 = 1024$ pixels [8].

Due to their low kinetic energy, the radium ions were deposited close to the surface of the detector, i.e., within the first few tens of atomic layers of the dead-layer material, rather than being implanted in the sensitive silicon detector volume. This implies various effects on the measured particle spectra:

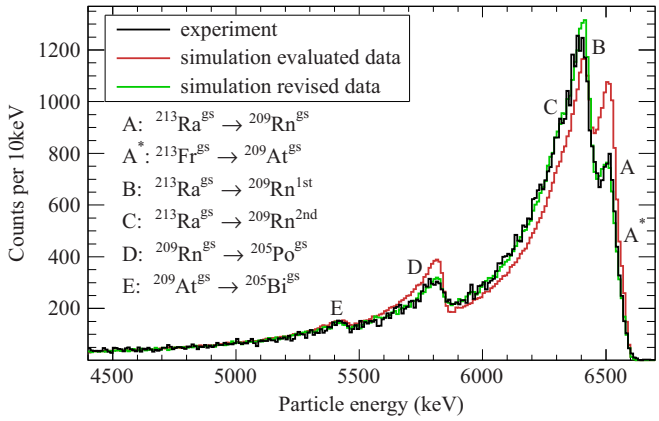

FIG. 3. The experimentally observed particle spectrum (black) compared with the simulation using evaluated (red) and revised (green) α-branching ratios. Using the evaluated α-branching ratios, the α peaks labeled A, A^*, and D are significantly overestimated. By adjusting α-branching ratios in the ^{213}Ra decay path, the experimentally observed spectrum can be reproduced accurately. See text for details.

(1) α particles have to traverse the whole dead layer to reach the active detector volume, leading to very pronounced left tails on the α peaks (see Fig. 3). This significantly affects the effective resolution.
(2) If the α decay of ^{213}Ra is registered in the DSSSD, the daughter recoil has sufficient kinetic energy to fly off the surface of the DSSSD and either travel to one of the SSSSDs or leave the silicon cube at backward angles.
(3) Implantation-decay correlation is not possible, simply because there is no detectable implantation signal.

At the time of the experiment, the silicon box was inside a vacuum chamber fabricated of 0.5 mm thin stainless steel. In addition, two composite γ-ray detectors were engaged: One former EUROBALL cluster detector [31] was positioned 20 mm behind the DSSSD, slightly off center, and one VEGA clover detector [32] placed 15 mm behind one of the SSSSD, implying the use of a total of $7 + 4 = 11$ large-volume, high-purity germanium crystals for γ- and x-ray detection.

The present data set originates from a measurement which lasted for about 15 hours. List-mode events were generated by a GSI-MBS [33] data acquisition system driving a single VME crate, which comprised standard modules to digitize the energies and the times of the silicon and germanium detectors. The MBS system was triggered by either (i) a release signal from SHIPTRAP, (ii) signals from either a DSSSD or SSSSD strip in excess of a threshold energy of $\sim$500 keV, or (iii) a germanium detector signal corresponding to at least $\sim$30 keV in energy. The latter trigger was only used for energy and efficiency calibration purposes, conducted with standard γ-ray sources of ^{133}Ba and ^{152}Eu. The silicon detectors were calibrated with three- and four-line α sources containing ^{233}U, ^{239}Pu, ^{241}Am, and ^{244}Cm, before and after the in-beam setting. During the experiment, the basic functioning of the TASISpec system could also be monitored with a ^{241}Am source mounted onto the same movable rod as the MCP detector, i.e., located at the entrance of the focusing tube (cf. Fig. 2) when deemed necessary.

Following a careful energy calibration and time alignment of the various detector channels, the data were sorted offline into various one-dimensional spectra and two-dimensional correlation matrices. In particular, correlations between the DSSSD and germanium-detector energies as well as SSSSD and germanium-detector energies were studied. For these, an energy-dependent prompt coincidence time window between the triggering silicon-detector channel and the coincident germanium-detector event was implemented, reaching from about 700 ns at 30 keV down to 100 ns at and beyond 1 MeV. To avoid events where particles interacted in the inter-strip region of the DSSSD, only events with the same energy deposition in the n-side and p-side strips were considered for the analysis. So-called nearest neighbor add-back was performed for the composite germanium detectors: i.e., the energies of neighboring crystals were summed upon (i) prompt coincidence, (ii) a minimum sum energy of 200 keV, and (iii) a minimum individual energy of 30 keV.

III. GEANT4 SIMULATION

A virtual TASISpec setup encoded with the GEANT4 simulation framework [34] is available [35]. Differences between the present so-called "TRAPSpec" (this work) and the full TASISpec setup can easily be accounted for. This includes, for instance, the exact location and type of germanium detectors, silicon-detector thicknesses, and their segmentation. The accuracy of the implementation was crosschecked by reproducing the spectra obtained from the calibration runs with ^{133}Ba, ^{152}Eu, and the four-line α source. With the proper virtual setup defined, a fully time-resolved simulation of the experiment was conducted:

As in the experiment, 2-keV $^{213}Ra^{2+}$ ions in the ground state were sent at a rate of 2.5 Hz towards the DSSSD such that

(1) the observed beam profile, i.e., the DSSSD hit pattern of subsequent ^{213}Ra α decays, reproduces the experimentally observed one,
(2) ^{213}Ra and its daughter activity is built up as in the real experiment, and
(3) the statistics of experiment and simulation match.

The produced list-mode data comprising energies and times of each detected event is treated with the identical offline analysis procedure as the original, experimental data set. This scheme allows for a direct comparison of observed and simulated spectra.

Besides the definition of the experimental setup, the second major input for the simulation is tabulated nuclear decay data. The starting point for the present GEANT4 (version 10.01.p02) study are databases for radioactive decay (version 4.2) and photon evaporation (version 3.1) [34]. For each nuclear quantum state, these files specify experimental observables such as decay type, half-life, decay energies, decay branches, conversion coefficients, etc. The spectra derived from a simulation can then be confronted with the actual experimental results. Adjustments in the database may be needed to account

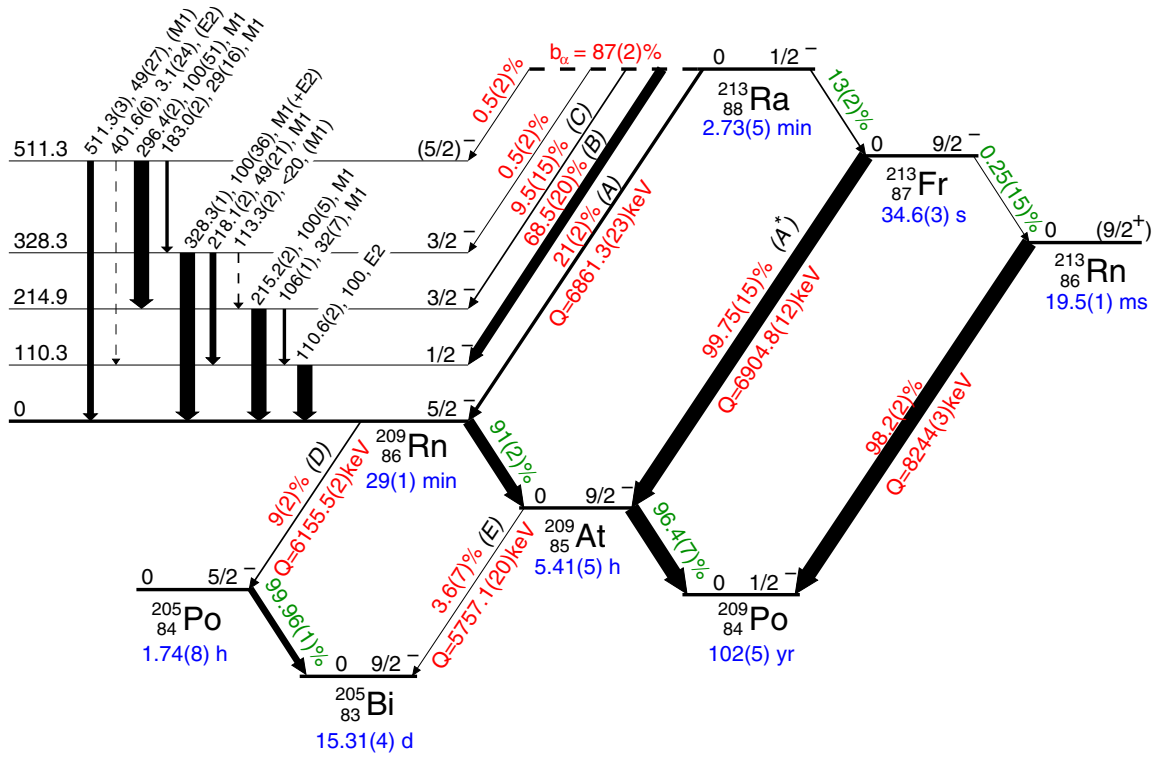

FIG. 4. Adopted decay scheme of the ^{213}Ra ground-state decay path based on the revised decay data from this work. This concerns mostly the relative α/EC-branching ratio of the ^{213}Ra ground state and its relative α-decay branching ratios to ^{209}Rn (compare also to Fig. 1). The values for the transitions from the states at 328 and 511 keV are adopted from [13], except for the relative γ-ray intensity of the 113 keV transition [21]. α-decay branching ratios and Q values are presented in red, β^+/EC-decay branching ratios in green. The six α-decay branching ratios labeled A to E are identified as peaks in Fig. 3. The α-decay branching ratios A, B, and C are compared to theoretical calculations in Sec. V. Further details are presented in the text.

for inconsistencies between simulation and measurement. This requires a well-understood detector system and experimentally clean conditions: Here, the separation of the nuclear ground state of ^{213}Ra by SHIPTRAP is *the* mandatory prerequisite.

IV. RESULTS: CONFRONTING SIMULATION WITH EXPERIMENT

Simulating the conducted experiment using evaluated data (see Fig. 1 and Table I) and comparing the resulting particle spectrum with the experimentally observed one reveals significant discrepancies. As is clearly visible in Fig. 3, the intensity of the peak labeled $A^{(*)}$ (comprising the ground-state to ground-state α decays from ^{213}Ra to ^{209}Rn, A, and ^{213}Fr to ^{209}At, A^*) is significantly overestimated by the evaluated data. Starting off from this discrepancy, at first relevant α-branching ratios and then relative γ-ray intensities are adjusted until experimental and simulated results are in good agreement.

This procedure is discussed in more detail in Ref. [30]. In short, every parameter (e.g., α-branching ratios, relative γ-ray intensities, or transition multipolarities) was varied and for each variation a new simulation was conducted. The resulting particle and photon spectra were then compared to the experiment by means of a χ^2 test. Furthermore, since the total number of ^{213}Ra ions that left the trap and reached the decay station is known, the yield in the observed spectra must be reproduced by the simulation without any additional normalization. The values of the parameter set which fulfill both criteria best (minimal χ^2 and congruent spectra yields) are shown in Fig. 4 and discussed in the following.

In general, this work is primarily sensitive to α-branching ratios, whereas a variation in relative γ-ray intensities does not allow one to further constrain evaluated data because of limited statistics.

A. ^{213}Ra

Due to the shallow deposition of the ^{213}Ra ions, the α peak at 6.5 MeV in Fig. 3 from the ^{213}Ra decay to the ^{209}Rn ground state becomes a doublet with the ^{213}Fr α peak, having only 43 keV energy difference. Due to energy summing of α particles and conversion electrons, also the α decay of the ^{213}Ra ground state to the first excited state of ^{209}Rn contributes to this peak (for a more detailed discussion see Sec. IV E). However, evaluating the peak shape and intensity of this peak by comparing the experimental spectrum to simulations with different α-branching ratios as described in Ref. [30], it is possible to deduce rather well defined α-branching ratios: a total ^{213}Ra α-branching ratio of 87(2)% and a relative α-branching ratio of 21(2)% to the ^{209}Rn ground-state is needed to reproduce the same intensity and peak shape (see Fig. 3); i.e., these values lead to the minimal χ^2 value. The

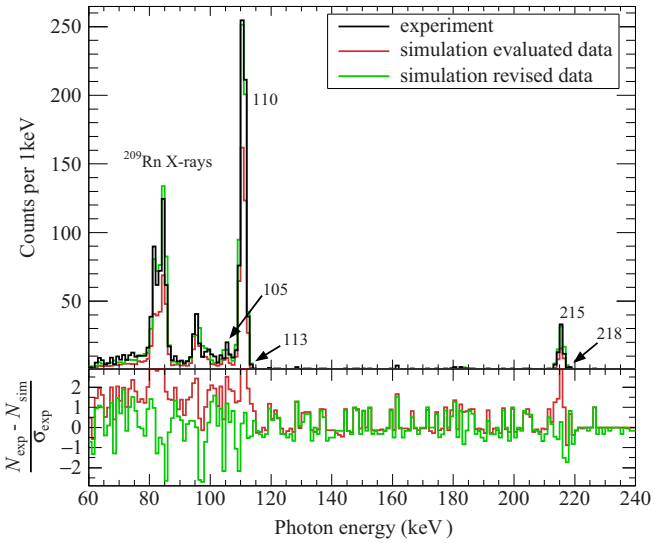

FIG. 5. Comparing the experimentally observed photon spectrum (black) with the simulation using evaluated (red) and revised (green) relative γ-ray intensities, multipolarities, and α-branching ratios (see also Fig. 4). Due to the underestimated α-branching ratios to the excited states of ^{209}Rn, the photon spectrum has a too low yield when using evaluated data.

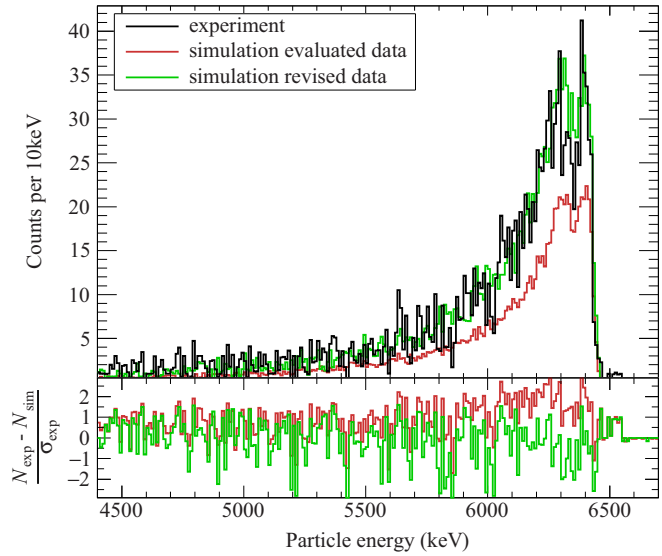

FIG. 6. The particle-photon coincidence spectrum observed in the experiment (black) compared with the result from the simulation using evaluated (red) and revised (green) decay data. As in the case of the photon spectrum (Fig. 5), the yield is too low when using evaluated decay data because of the underestimated α-branching ratios to the excited states of ^{209}Rn.

former value differs by 7% from the previously estimated value of 80(5)% [10]. Most importantly, the revised relative α-branching ratio to the ^{209}Rn ground state is nearly half of the previously reported value of 45.5(17)% [13]. As mentioned earlier, the evaluated value dates back to the first measurements from Refs. [10,19]. Both used a very similar apparatus where the activity is placed in front of a 25 mm^2 surface-barrier detector [10,36] or an annular detector [19,37]. It seems likely that both measurements equally suffered from energy summing (see also Sec. IV E) and that the difference in the obtained relative α-branching ratio to the ^{209}Rn ground-state can be attributed to this effect.

Because of the much smaller α-branching ratio to the ^{209}Rn ground-state and the larger total α-branching ratio of ^{213}Ra, the relative α-branching ratios to the excited states of ^{209}Rn are larger, especially to the first excited state. Since the deexcitation of these states is the only source of γ rays, the yield in the photon and particle-photon coincidence spectra increases accordingly, leading to much better agreement with the experimental observations (see Figs. 5–8, respectively). Assuming the adjusted α branching to the 328 keV state and the established 328 and 218 keV ($M1$) γ-ray transitions leads to rather well reproduced intensities in the photon spectrum. However, including the 113 keV transition suggested by Kuusiniemi *et al.* [21] lowers—depending on its relative γ-ray intensity and multipolarity—the yields of the other transitions, therefore implying an enhanced α-branching ratio to the 328 keV state. According to Ref. [21] the relative γ-ray intensity of such a transition has an upper limit of 15% and has most likely multipolarity $M1$. By implementing this 113 keV transition, the relative α-branching ratio to the 328 keV state must be increased to 0.5(2)% in order to obtain a consistent photon spectrum. Although the effect of this larger α-branching ratio is not directly apparent by looking at the particle spectrum, its χ^2 value improves by implementing this transition, supporting the presence of such a transition.

B. ^{213}Fr and ^{213}Rn

^{213}Fr decays via its β^+/EC branch to ^{213}Rn which is short-lived and α-decays 100% to ^{209}Po [13]. The relative branching ratio for the ^{213}Rn ground-state to ground-state α decay is

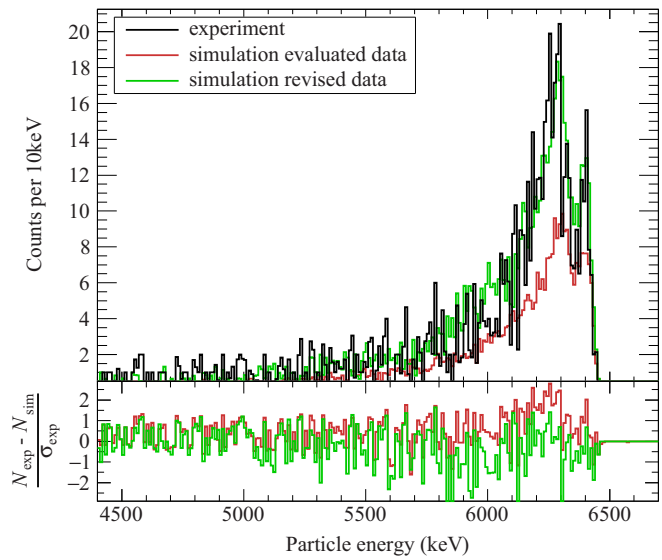

FIG. 7. The particle spectrum in coincidence with x-rays observed in the experiment (black) compared with the result from the simulation using evaluated (red) and revised (green) decay data. See text for more details.

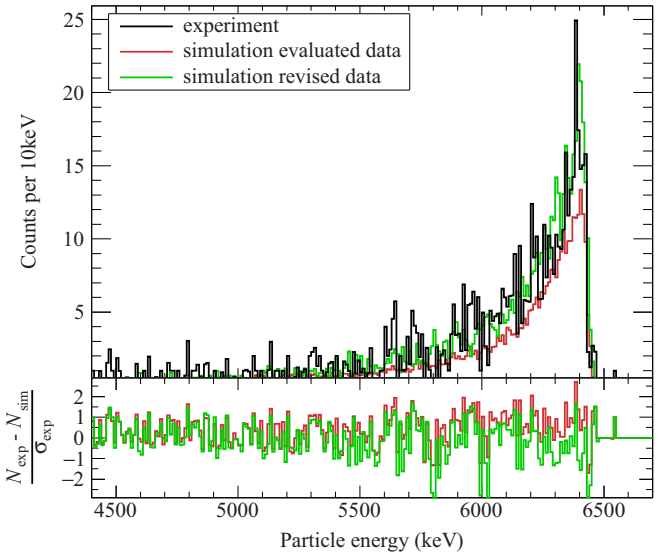

FIG. 8. The particle spectrum in coincidence with the 110 keV γ-ray observed in the experiment (black) compared with the result from the simulation using evaluated (red) and revised (green) decay data. See text for more details.

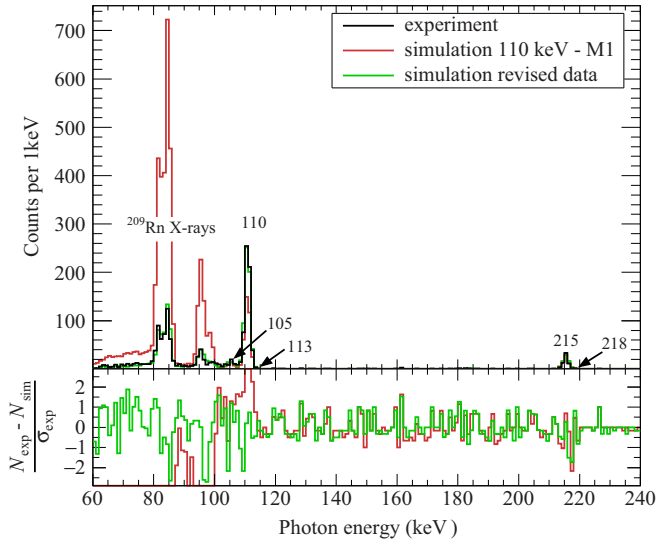

FIG. 9. Changing the multipolarity of the 110 keV transition from $E2$ to $M1$ (red) overestimates the x-ray yield and underestimates the 110 keV γ-peak yield excessively. Using the evaluated $E2$ multipolarity instead (green) reproduces the experiment (black) very well, supporting the established multipolarity assignment.

98.2(2)% and has an α energy of 8089 keV. This is 1.3 MeV larger than the ^{213}Fr α energy and therefore the highest particle energy in the ^{213}Ra decay path. Hence, the ^{213}Rn α peak is well separated and does not suffer from overlap with tails from other peaks. Any α particle detected with a higher energy than the ^{213}Fr α energy can be attributed to the ^{213}Rn α decay. Assuming a well characterized ^{213}Rn decay in the evaluated data, the observed intensity of its 8089 keV α peak enables conclusions about the ^{213}Fr β^+/EC-branching ratio.

Despite the limited statistics for the ^{213}Rn α decay, it is possible to deduce a branching ratio of 0.25(15)% for the β^+/EC decay of ^{213}Fr. This value is significantly lower than previous estimates of 0.52(3)% [16], 0.57(3)% [38], and 0.9(1)% [17].

As already discussed in Ref. [17] a common problem in determining the α-β^+/EC-branching ratio is that radon is a noble gas and does not stick to surfaces and might diffuse out of the detector material. Hence, some of its α activity might be lost if the ^{213}Rn -ion is not implanted deep enough into the silicon detector, which could explain the large differences in the measured β^+/EC branchings (see also discussion in IV C). Such effects are not treated within the GEANT4 simulation.

C. ^{209}Rn

Using the established ^{209}Rn level scheme [13,21] as input for the simulation leads to, by and large, consistent results. A relative γ-ray intensity of <20% for the 113 keV transition is also consistent with the experimental measurement. As described in Sec. IV A, including this transition leads to slightly improved χ^2 values.

Assuming pure multipole transitions as listed in Table I leads to the best agreement, supporting previous spin-parity assignments for the low-lying states in ^{209}Rn. Using different multipolarities as input for the simulation results in either overestimated γ-ray yields and an underestimated x-ray yield or vice versa. In turn this would also lead to inconsistent yields in particle-photon coincidence spectra. This holds true especially for the most intense transitions, i.e., the 110, 105, and 215 keV transitions. In Fig. 9 the 110 keV transition was assumed to be purely $M1$, resulting in significant discrepancies with the experiment. Similarly, an $E2$ multipolarity was assumed for the 105 keV transition in Fig. 10. Once again, the experimental results cannot be reproduced. When changing

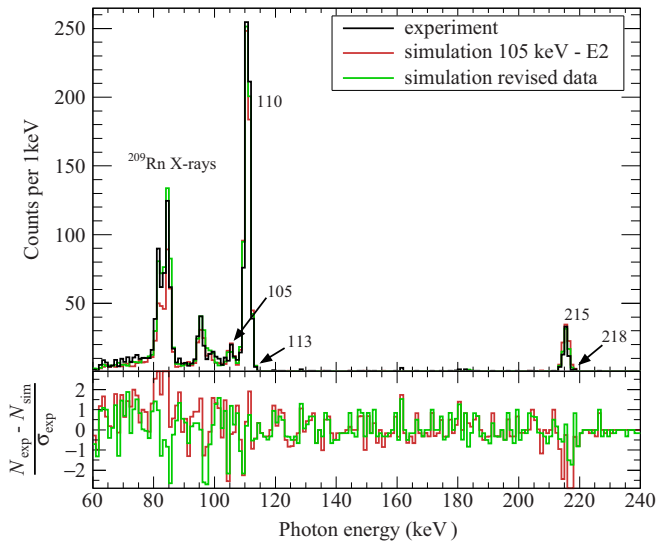

FIG. 10. Similarly to Fig. 9, the 215 keV γ-peak yield is overestimated and the x-ray yield significantly underestimated when changing the multipolarity of the 105 keV transition to $E2$ (red). Much better agreement with the experimental results (black) is obtained when assigning an $M1$ multipolarity instead (green).

the multipolarity of the 215 keV transition to $E2$, the yield in the corresponding particle-photon coincidence spectrum is significantly overestimated. Therefore, this work supports the assignment of pure multipole transitions as stated in Table I. For transitions deexciting the third or fourth excited state, the statistics are too low to obtain conclusive results on their multipolarities. The assumed multipolarities from Table I, however, do not imply any inconsistencies.

The α-branching ratio of ^{209}Rn can be determined to be 9(2)%. This value is not consistent with the evaluated value of 17(2)%, but as already discussed in Sec. IV B, the measurement might suffer from lost activity due to radon being a noble gas. Since the half-life of ^{209}Rn is sufficiently long, $T_{1/2} = 29(1)$ min, and the ^{213}Ra ions are very shallowly deposited, it is likely that ^{209}Rn activity is lost because it diffuses out of the detector material. While our GEANT4 simulations considered a loss because of the ^{209}Rn recoil after the ^{213}Ra decay, diffusion was not implemented in the simulations, and hence neglected.

For a first estimation of the magnitude of diffusion losses Fick's diffusion laws were employed. As the beam size with a cross section of about 1.25 cm^2 is large relative to the width of the implanted radium distribution along the beam axis z, we assume the concentration to be constant in the x-y plane (parallel to the detector surface). This reduces the diffusion problem to a one-dimensional case. After roughly five hours of experiment time, ^{213}Ra and ^{209}Rn are in radioactive equilibrium. In this case we can assume a constant ^{213}Ra distribution in time and Ficks first law can be applied. The ^{213}Ra distribution has been estimated with SRIM [39] and follows a narrow Gaussian profile with a standard deviation of only 1.0 nm and the maximum at 6.8 nm below the detector surface. From the simulated recoil the standard deviation of the ^{209}Rn distribution after the decay was deduced as 28.8 nm. As the estimation for this static case suggests that more ^{209}Rn is lost by diffusion than is actually produced, it raises the question whether the ^{209}Rn concentration is static in time.

Unfortunately, the complexity of the problem did not allow for quantitative results. Furthermore, the diffusion constant of Rn in SiO_2—the dead-layer material—is unknown and could only be estimated from measurements in similar materials. Hence, an exact solution cannot be easily deduced. The expected value of the Gaussian distribution of the Rn atoms, however, is unaffected by a nonstatic concentration, as the ^{209}Rn is always produced in the same depth of the detector, maintaining the concentration maximum in this area. Due to the close proximity of this main fraction of atoms to the detector surface, it is suggested that about 50% are lost by diffusion. This effect can readily explain the discrepancy in the expected ^{209}Rn activity.

Note that the yield and shape of the ^{209}Rn photon spectrum is unaffected by any diffusion loss, since the deexcitation inside the ^{209}Rn nucleus happens in prompt coincidence with the ^{213}Ra α decay.

D. ^{209}At

Rather independently of other branching ratios in the ^{213}Ra decay chain, the ^{209}At α intensity could be best reproduced by using an α-decay branching ratio of 3.6(7)%. This value is compatible with the hitherto reported value of 4.1(6)%. Note that ^{209}At is produced by the ^{213}Fr α decay as well as the ^{209}Rn β^+/EC decay. Therefore this value might be also affected by the loss of radon activity as discussed in Secs. IV B and IV C.

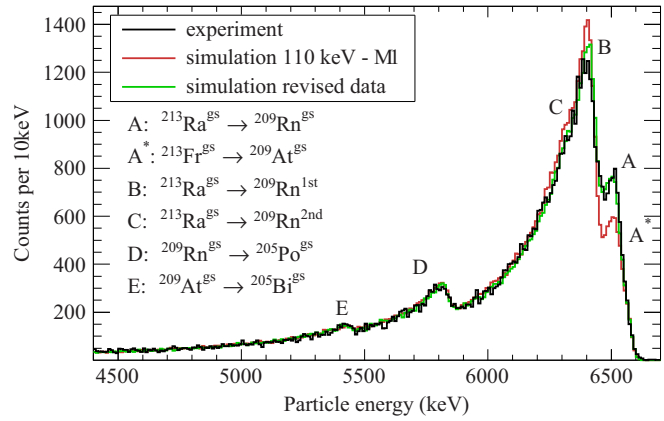

FIG. 11. Particle spectrum corresponding to the photon spectrum shown in Fig. 9, exemplifying the impact of energy summing of α particles, conversion electrons, and Auger electrons. See text for more details.

E. Remaining remarks

As is evident from the spectra in Figs. 3, 5, and 6, the spectra shapes and yields of particle, photon, as well as coincidence spectra could be reproduced very well within statistical fluctuations. This has been achieved by primarily adjusting α-decay branching ratios.

Furthermore, setup-related parameters, such as HPGe-detector positions and the dead-layer thickness of the DSSSD, which have not been precisely measured or determined prior to this study, have been varied within their uncertainties to study their effect on the resulting branching ratios. Due to the large number of parameters and their correlations, it proved to be very difficult to conduct a fully comprehensive multiparameter error analysis. Stated uncertainties in this work are guided by the change of the χ^2 value due to changes of the corresponding parameter in the simulation and by variations of setup-related parameters. For every set of input parameters, the simulation is carried out several times with different random number seeds, leading to distributions in the observables reflecting their statistical significance.

An important aspect when studying α decays in the heavy and superheavy element region is the energy summing of α particles, conversion electrons, and Auger electrons in cases where the daughter nucleus is in an excited state after the α decay. This issue and its implications on measured α-decay branching ratios are discussed in detail in, e.g., Refs. [40,41]. Although this effect is not avoided in the present experiment, it is taken into account by the simulation: Fig. 11 is the particle spectrum corresponding to the photon spectrum shown in Fig. 9, where the multipolarity of the 110 keV transition, $E2$, in ^{209}Rn is changed to $M1$. There the effect is nicely

TABLE II. Conversion coefficients α for the 110 keV transition in ^{209}Rn assuming a multipolarity of $E2$ or $M1$. The presented values for the conversion-electron energies E_{CE} are for an $E2$ transition but are very similar for a $M1$ transition. Values are taken from Ref. [23].

Shell	E_{CE} (keV)	$E2$	$M1$
Total		5.54(8)	10.01(14)
K	11.60	0.362(5)	8.07(12)
L	93.75	3.82(6)	1.476(21)
M	106.11	1.030(15)	0.351(5)
N	109.12	0.268(4)	0.0914(13)

demonstrated: For an $M1$ transition mostly K conversion is present, leading to conversion-electron energies of about 10 keV. An $E2$ transition, however, has mostly L and M conversion with conversion-electron energies of about 90 and 100 keV (see Table II). Hence, the energy summing of a L or M conversion electron and the α particle from the ^{213}Ra ground-state α decay into the first excited state of ^{209}Rn will lead to an enhanced yield of the α peak from the ^{213}Ra ground-state to ground-state α decay. Since the distance between the decaying ^{213}Ra ions and the detector—i.e., the dead-layer thickness of $\sim$2 μm—is much smaller than the pixel size of $\sim$1.9 mm, the probability of energy summing is very high.

Obviously the magnitude of the energy summing depends strongly on the transition properties (transition energy, multipolarity, and half-life) and the geometry of the setup, such as source-to-detector distance, dead-layer thickness, and depletion depth of the detector, or, in the case of implantation of the investigated nuclei into the detector, the implantation depth. Hence, this feature is difficult to assess with analytical methods. However, a complete simulation of the physical process and the detector geometry with, e.g., GEANT4 allows for accurate treatment of the energy summing (see, e.g., Ref. [41]).

Currently GEANT4 does not include angular correlations between α particles and γ rays or conversion electrons, which might have a minor effect on the relative γ-ray intensities and α-branching ratios. However, the dominating intensities in the particle and photon spectra stem from decays to and from the first excited state at 110 keV in ^{209}Rn and from ground-state to ground-state α decays. Since the 110 keV state in ^{209}Rn has a spin of $I = 1/2$, all consecutive decays populating and depopulating that state have no angular correlation. Therefore, the impact on the result from neglecting angular correlation in the simulation is expected to be negligible.

V. THEORETICAL INTERPRETATION

With only seven valence particles and holes, ^{209}Rn and ^{213}Ra are close to the doubly magic ^{208}Pb nucleus. As expected, standard Nilsson-Strutinsky calculations [42] predict both ^{209}Rn and ^{213}Ra to be spherical. The Lublin-Strasbourg drop parametrization [43] for the liquid drop energy and Rozmej parameters, which have been fitted in the actinide region [44,45], for the strength of the $\vec{l}\cdot\vec{s}$ and l^2 couplings were used. In Fig. 12 the calculated total energy surface for ^{209}Rn is shown.

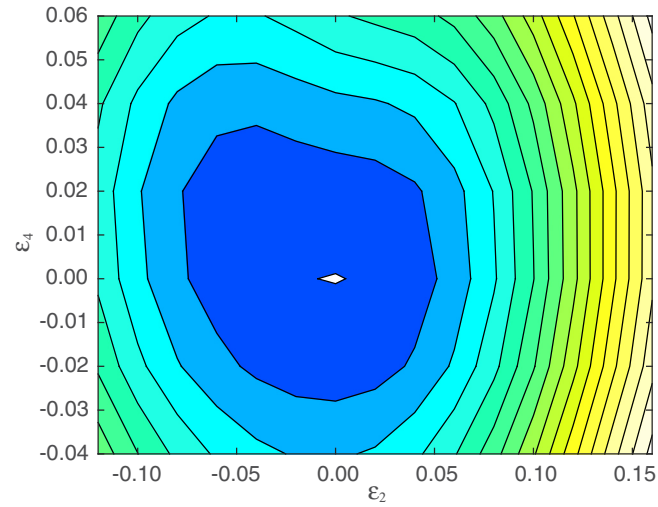

FIG. 12. Total energy surface for ^{209}Rn. The minimum is clearly centered around $\varepsilon_2 = \varepsilon_4 = 0$, predicting ^{209}Rn to be spherical. The contour line separation is 0.5 MeV.

This enables the calculation of α-decay rates for ^{213}Ra as described in Ref. [46], which assumes spherical nuclei. The "surface pairing" effective pairing interaction employed in Ref. [46] is used. States in even-Z–odd-N nuclei connected by α decay are described as single quasineutron excitations of an even-even Hartree-Fock-Bogoliubov vacuum. The ground state of the mother nucleus ^{213}Ra and the three lowest lying states in the daughter ^{209}Rn are assumed to have the quasiparticle structure shown in Table III. The Coulomb penetrability is evaluated using the experimental Q_α values.

The decay rates $\lambda = b_\alpha I \ln(2)/T_{1/2}$, where b_α is the α-branching ratio, I the intensity within the α-decay branch, and $T_{1/2}$ the half-life, for the three channels are listed in Table IV. The sum of the theoretical intensities $I_{\rm th}$ for the three channels is normalized to 100%, neglecting the small branching ratios to higher-lying states.

The theoretical rate and branching ratio for channel A, described as a hindered decay where the odd neutron changes orbital from $p_{1/2}$ to $f_{5/2}$, and for channel B, a favored decay where the odd neutron remains in the same orbital, agree much better with the revised branching ratio than with the previous data. On the other hand, in the calculations the decay rate for the spin-flip $p_{1/2} \rightarrow p_{3/2}$ decay, C, becomes smaller than in experiment.

TABLE III. α-decay channels for the ^{213}Ra decay to ^{209}Rn considered in the theoretical calculations: the ground-state to ground-state decay A, the ground-state decay to the first excited state B, and to the second excited state C (compare to Fig. 4). The assumed odd-neutron quasiparticle configurations are shown in the rightmost column.

Channel	$I_i^\pi \rightarrow I_f^\pi$	Neutron q.p.
A	$1/2^- \rightarrow 5/2^-$	$p_{1/2} \rightarrow f_{5/2}$
B	$1/2^- \rightarrow 1/2^-$	$p_{1/2} \rightarrow p_{1/2}$
C	$1/2^- \rightarrow 3/2^-$	$p_{1/2} \rightarrow p_{3/2}$

TABLE IV. Comparison between evaluated and revised data, and theoretical calculations for the α decay of ^{213}Ra. The leftmost column indicates the decay channel; see Table III. Q_{exp} are the corresponding Q values, I the relative α-decay branching ratios, and $\lambda = b_\alpha I \ln(2)/T_{1/2}$ the decay rates.

Ch.	Q_{exp} (MeV)	I_{exp} [a]	I_{exp} [b] (%)	I_{th}	λ_{exp} [a]	λ_{exp} [b] (10^{-3} s^{-1})	λ_{th}
A	6.861	45.5(17)	21(2)	24.0	1.54(12)	0.78(8)	0.852
B	6.751	48.5(17)	68.5(20)	71.7	1.64(12)	2.52(7)	2.55
C	6.646	5.8(6)	9.5(15)	4.3	0.196(24)	0.35(6)	0.155

[a]Evaluated decay data (i.e., Fig. 1).
[b]Revised decay data (i.e., Fig. 4).

In order to validate the assumption of the pure quasiparticle configurations listed in Table III, shell-model calculations have been performed using the code NUSHELLX [49,50]. Besides ^{213}Ra and ^{209}Rn, other odd-mass nuclei with $N = 125$ and $N = 123$ have also been considered to gain confidence in the results of the conducted shell-model calculations. To access the series of $N = 123$ and $N = 125$ nuclei located "northwest" of ^{208}Pb in the chart of nuclides, a residual proton particle and neutron hole interaction denoted "pbpop" [47] was employed, while fixing ^{208}Pb as a closed core.

The active model space thus comprises the single proton orbitals $1h_{9/2}$, $2f_{7/2}$, and $1i_{13/2}$, as well as neutron holes in the orbitals $1i_{13/2}$, $3p_{3/2}$, $2f_{5/2}$, and $3p_{1/2}$. For the α-decay mother/daughter pairs ^{209}Po/^{205}Pb, ^{211}Rn/^{207}Po, and ^{213}Ra/^{209}Rn no further truncation is required. However, for the pair ^{215}Th/^{211}Ra the maximum number of protons in the $2f_{7/2}$ and $1i_{13/2}$ orbitals had to be restricted to two each, implying a maximum number of four protons being excited out of the underlying $1h_{9/2}$ orbital. This truncation is found necessary due to rapidly increasing dimensions in the shell-model matrix diagonalization routines. The summed average proton occupation number in the $2f_{7/2}$ and $1i_{13/2}$ orbitals is found to be about 1 for the low-lying states of interest; i.e., the truncation is not expected to lead to any major change of the predictions relevant for the present α-decay study.

It is also interesting to note that, due to these quickly increasing dimensions, the number of systematic large-scale shell-model surveys in the four quadrants around ^{208}Pb remains rather scarce as of today. In Ref. [51] the $N = 126$ series above ^{208}Pb was tackled, while Ref. [48] provides a recent attempt at a comprehensive shell-model description of the nuclei of interest (see Fig. 13).

In accordance with the experimental knowledge on the $N = 125$ isotones ^{209}Po, ^{211}Rn, ^{213}Ra, and ^{215}Th, their α-decaying ground states are predicted to have spin-parity $I^\pi = 1/2^-$. Beside BCS-like pair fluctuations of $S = 0$ nucleon pairs, the ground-state wave functions are dominated by expected single neutron hole $3p_{1/2}^{-1}$ configurations, with the respective partitions ranging from 97% in ^{209}Po to 94% in ^{215}Th. These numbers clearly support the pure quasiparticle configuration of the ^{213}Ra ground state used in the α-decay rate calculations mentioned earlier. In addition, the shell-model predictions for

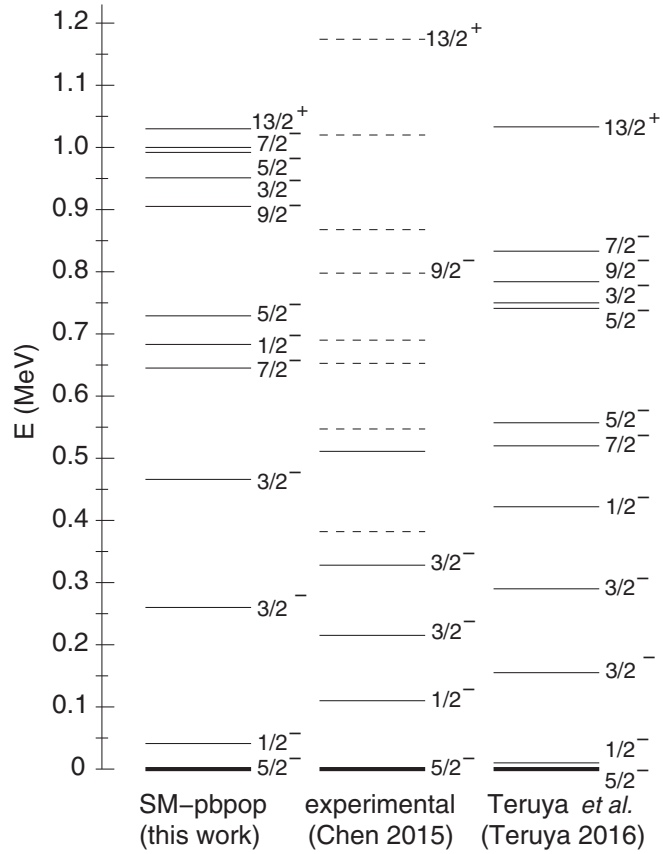

FIG. 13. The experimental [13] energy spectrum for ^{209}Rn in comparison with theoretical calculations. Next to the experimentally observed energy spectrum, the results of our shell-model calculations (SM-pbpop [47]) and those from the work of Teruya *et al.* [48] for all states up to the $13/2^+$ isomer are presented. The experimentally observed states not populated by the α decay of the ^{213}Ra ground state are dashed. Only evaluated spin-party assignments are presented. See text for more details.

the low-lying negative-parity as well as medium-spin states are found to be in very good agreement with the experimental observations: Mean-level deviations are below 50 keV, and the yrast $17/2^-$ level in ^{211}Rn is correctly predicted as an isomeric state, to name a specific example.

Similarly, both the observed negative-parity low-spin sequence $5/2^-$, $1/2^-$, $3/2^-$, $3/2_2^-$ as well as the position of the $13/2^+$ isomers in the $N = 123$ daughter series ^{205}Pb, ^{207}Po, ^{209}Rn, and ^{211}Ra are very well reproduced in the shell-model calculations. The predictions for ^{209}Rn are included in Fig. 13. Here, the wave functions of the yrast negative-parity states relevant for the α-decay branching calculations are predicted to be rather pure neutron hole states as well: For instance, in ^{209}Rn the respective partitions sum up to 86% ($5/2^-$ ground state, $2f_{5/2}$), 88% ($1/2^-$ state, $3p_{1/2}$), and 82% ($3/2^-$ state, $3p_{3/2}$). The corresponding numbers are about 5% higher (lower) for ^{207}Po (^{211}Ra); i.e., they decrease as a function of distance from the ^{208}Pb core, as expected. This, again, supports the approach of the α-decay rate calculations. The fact that the single-particle partitions are rather similar for all single-particle states in a given $N = 123$ isotone implies

insignificant modifications to the theoretical *relative* α-decay branchings listed in Table IV.

The fact that the conducted shell-model calculations provide rather consistent results for the considered odd-mass nuclei with $N = 123$ and $N = 125$ suggests that the obtained single-particle partitions are reliable.

VI. SUMMARY AND OUTLOOK

The ^{213}Ra decay path has been exclusively studied by utilizing SHIPTRAP's mass resolving power in combination with the nuclear decay station TASISpec and contemporary GEANT4 simulations. By adjusting the ^{213}Ra decay data it was possible to reproduce the experimental results in a virtual GEANT4 experiment. The resulting ^{213}Ra decay data has been presented and discussed, calling for a revision of the ^{213}Ra α-decay branching ratios. These findings are supported by theoretical calculations. The assumptions used in the calculation of the ^{213}Ra α-decay branching ratios are justified by standard Nilsson-Strutinsky and shell-model calculations. Altogether, this work shows the potential of GEANT4-aided quantum-state-selective decay spectroscopy.

Due to the selection of a single nuclear state, the presented method has major advantages compared to standard isotope selection schemes. The experimental scheme is background free and the composition of the incoming beam is very easily and accurately simulated. Furthermore, the virtual simulation of the experiment intrinsically captures detector effects and correlations between observables, which are often difficult to access otherwise. Therefore, this method has the potential to advance the precision level of decay spectroscopy of heavy elements, $N \sim Z$ nuclei, and rp-process waiting point nuclei, to name but a few. Even technological aspects, when precise actinide decay branches for radioactive waste disposal and/or new fuel cycles of generation IV nuclear reactors are of interest [52], can be a useful field to apply GEANT4-aided quantum-state-selective decay spectroscopy.

ACKNOWLEDGMENTS

The authors would like to thank the staff and the accelerator crew at GSI. Support from the GSI Summer Student Program 2009 is gratefully acknowledged. This work is supported in part by the Swedish Research Council (Grants No. VR 2011-5253 and No. VR 2013-4271), the Knut and Alice Wallenberg Foundation (Grant No. KAW 2015.0021), the Royal Physiographic Society in Lund, and the German Federal Ministry of Education and Research BMBF (Grants No. 05P15HGFNA, No. 05P12HGFN5, and No. 05P09HGFN5).

[1] L. Weissman, F. Ames, J. Äystö, O. Forstner, K. Reisinger, and S. Rinta-Antila, Nucl. Instrum. Methods Phys. Res., Sect. A **492**, 451 (2002).
[2] J. Rissanen, J. Kurpeta, A. Plochocki, V.-V. Elomaa, T. Eronen, J. Hakala, A. Jokinen, A. Kankainen, P. Karvonen, I. D. Moore *et al.*, Eur. Phys. J. A **47**, 97 (2011).
[3] J. Rissanen, J. Kurpeta, V.-V. Elomaa, T. Eronen, J. Hakala, A. Jokinen, I. D. Moore, P. Karvonen, A. Plochocki, L. Próchniak *et al.*, Phys. Rev. C **83**, 011301(R) (2011).
[4] S. Rinta-Antila, T. Eronen, V.-V. Elomaa, U. Hager, J. Hakala, A. Jokinen, P. Karvonen, H. Penttilä, J. Rissanen, T. Sonoda, A. Saastamoinen, and J. Äystö, Eur. Phys. J. A **31**, 1 (2007).
[5] M. Kowalska, S. Naimi, J. Agramunt, A. Algora, D. Beck, B. Blank, K. Blaum, Ch. Böhm, Ch. Borgmann, M. Breitenfeldt *et al.*, Nucl. Instrum. Methods Phys. Res., Sect. A **689**, 102 (2012).
[6] J. Stanja, Ch. Borgmann, J. Agramunt, A. Algora, D. Beck, K. Blaum, Ch. Böhm, M. Breitenfeldt, T. E. Cocolios, L. M. Fraile *et al.*, Phys. Rev. C **88**, 054304 (2013).
[7] N. A. Althubiti, D. Atanasov, K. Blaum, T. E. Cocolios, T. Day Goodacre, G. J. Farooq-Smith, D. V. Fedorov, V. N. Fedosseev, S. George, F. Herfurth *et al.*, arXiv:1705.03546.
[8] L.-L. Andersson, D. Rudolph, P. Golubev, R.-D. Herzberg, R. Hoischen, E. Merchán, D. Ackermann, Ch. E. Düllmann, K. Eberhardt, J. Even *et al.*, Nucl. Instrum. Methods Phys. Res., Sect. A **622**, 164 (2010).
[9] M. Block, D. Ackermann, K. Blaum, A. Chaudhuri, Z. Di, S. Eliseev, R. Ferrer, D. Habs, F. Herfurth, F. P. Heßberger *et al.*, Eur. Phys. J. D **45**, 39 (2007).
[10] K. Valli, W. Treytl, and E. K. Hyde, Phys. Rev. **161**, 1284 (1967).
[11] Y. V. Lobanov and V. A. Durin, Yad. Fiz. **8**, 849 (1968) [Sov. J. Nucl. Phys. **8**, 493 (1969)].
[12] A. Rytz, At. Data Nucl. Data Tables **47**, 205 (1991).
[13] J. Chen and F. G. Kondev, Nucl. Data Sheets **126**, 373 (2015).
[14] N. A. Golovkov, S. Guetkh, B. S. Dzhelepov, Y. V. Norseev, V. A. Khalkin, and V. G. Chumin, Izv. Akad. Nauk SSSR, Ser. Fiz. **33**, 1622 (1969) [Bull. Acad. Sci. USSR, Phys. Ser. **33**, 1489 (1970)].
[15] N. A. Golovkov, R. B. Ivanov, A. Kolaczkowski, Y. V. Norseev, and V. G. Chumin, Izv. Akad. Nauk SSSR, Ser. Fiz. **35**, 2272 (1971) [Bull. Acad. Sci. USSR, Phys. Ser. **35**, 2063 (1972)].
[16] R. D. Griffioen and R. D. MacFarlane, Phys. Rev. **133**, B1373 (1964).
[17] P. Hornshøy, P. G. Hansen, and B. Jonson, Nucl. Phys. A **230**, 380 (1974).
[18] M. S. Basunia, Nucl. Data Sheets **108**, 633 (2007).
[19] D. G. Raich, H. R. Bowman, R. E. Eppley, J. O. Rasmussen, and I. Rezanka, Z. Phys. A **279**, 301 (1976).
[20] F. P. Heßberger, S. Hofmann, I. Kojouharov, and D. Ackermann, Eur. Phys. J. A **22**, 253 (2004).
[21] P. Kuusiniemi, F. P. Heßberger, D. Ackermann, S. Antalic, S. Hofmann, K. Nishio, B. Sulignano, I. Kojouharov, and R. Mann, Eur. Phys. J. A **30**, 551 (2006).
[22] F. G. Kondev, Nucl. Data Sheets **101**, 521 (2004).
[23] T. Kibédi, T. W. Burrows, M. B. Trzhaskovskaya, P. M. Davidson, and C. W. Nestor, Jr., Nucl. Instrum. Methods Phys. Res., Sect. A **589**, 202 (2008).
[24] D. Rudolph, M. Block, F. P. Heßberger, D. Ackermann, L.-L. Andersson, M. L. Cortes, C. Droese, M. Dworschak, M. Eibach, U. Forsberg *et al.*, in *GSI Scientific Report 2009*, GSI Report 2010-1, NUSTAR-SHE-08 (GSI, Darmstadt, 2010), p. 177.

[25] G. Münzenberg, W. Faust, S. Hofmann, P. Armbruster, K. Güttner, and H. Ewald, Nucl. Instrum. Methods Phys. Res., Sect. A **161**, 65 (1979).
[26] J. B. Neumayr, L. Beck, D. Habs, S. Heinz, J. Szerypo, P. G. Thirolf, V. Varentsov, F. Voit, D. Ackermann, D. Beck *et al.*, Nucl. Instrum. Methods Phys. Res., Sect. B **244**, 489 (2006).
[27] G. Savard, St. Becker, G. Bollen, H.-J. Kluge, R. B. Moore, Th. Otto, L. Schweikhard, H. Stolzenberg, and U. Wiess, Phys. Lett. **158**, 247 (1991).
[28] C. Droese, D. Ackermann, L.-L. Andersson, K. Blaum, M. Block, M. Dworschak, M. Eibach, S. Eliseev, U. Forsberg, E. Haettner *et al.*, Eur. Phys. J. A **49**, 13 (2013).
[29] U. Forsberg, D. Rudolph, P. Golubev, L. G. Sarmiento, A. Yakushev, L.-L. Andersson, A. Di Nitto, Ch. E. Düllmann, J. M. Gates, K. E. Gregorich *et al.*, Eur. Phys. J. Web Conf. **66**, 02036 (2014).
[30] C. Lorenz, L. Sarmiento, D. Rudolph, and M. Block, PoS (**INPC2016**) 073.
[31] J. Eberth, H. G. Thomas, P. V. Brentano, R. M. Lieder, H. M. Jäger, H. Kämmerfing, M. Berst, D. Gutknecht, and R. Henck, Nucl. Instrum. Methods Phys. Res., Sect. A **369**, 135 (1996).
[32] J. Gerl, H. Grawe, E. Roeckl, and H. J. Wollersheim, VEGA – A Proposal for Versatile and Efficient Gamma-detectors, GSI Darmstadt report, 1998 (unpublished).
[33] H. G. Essel and N. Kurz, IEEE Trans. Nucl. Sci. **47**, 337 (2000).
[34] S. Agostinelli, J. Allison, K. Amako, J. Apostolakis, H. Araujo, P. Arce, M. Asai, D. Axen, S. Banerjee, G. Barrand *et al.*, Nucl. Instrum. Methods Phys. Res., Sect. A **506**, 250 (2003).
[35] L. G. Sarmiento, L.-L. Andersson, and D. Rudolph, Nucl. Instrum. Methods Phys. Res., Sect. A **667**, 26 (2012).
[36] W. Treytl and K. Valli, Nucl. Phys. A **97**, 405 (1967).
[37] J. Borggreen, K. Valli, and E. K. Hyde, Phys. Rev. C **2**, 1841 (1970).
[38] K. Valli, E. K. Hyde, and W. Treytl, J. Inorg. Nucl. Chem. **29**, 2503 (1967).
[39] J. F. Ziegler, M. D. Ziegler, and J. P. Biersack, Nucl. Instrum. Methods Phys. Res., Sect. B **268**, 1818 (2010).
[40] F. P. Hessberger, S. Hofmann, G. Münzenberg, K.-H. Schmidt, P. Armbruster, and R. Hingmann, Nucl. Instrum. Methods Phys. Res., Sect. A **274**, 522 (1989).
[41] Ch. Theisen, A. Lopez-Martens, and Ch. Bonnelle, Nucl. Instrum. Methods Phys. Res., Sect. A **589**, 230 (2008).
[42] S. G. Nilsson, C. F. Tsang, A. Sobiczewski, Z. Szymański, S. Wycech, C. Gustafson, I.-L. Lamm, P. Möller, and B. Nilsson, Nucl. Phys. A **131**, 1 (1969).
[43] K. Pomorski and J. Dudek, Phys. Rev. C **67**, 044316 (2003).
[44] P. Rozmej, K. Boning, and A. Sobiczewski, in *Proceedings of the XXIV International Winter Meeting on Nuclear Physics, Bormio, Italy*, edited by I. Iori (Ric. Sci. Educ. Permanente, Milano, 1986), p. 567.
[45] C.-D. Herrmann, B. Prillwitz, V. Dämmrich, K. Freitag, P. Herzog, D. Mayer, K. Schlösser, and I. Ragnarsson, Nucl. Phys. A **493**, 83 (1989).
[46] D. E. Ward, B. G. Carlsson, and S. Åberg, Phys. Rev. C **92**, 014314 (2015).
[47] N. A. F. M. Poppelier and P. W. M. Glaudemans, Z. Phys. A **329**, 275 (1988).
[48] E. Teruya, K. Higashiyama, and N. Yoshinaga, Phys. Rev. C **93**, 064327 (2016).
[49] B. A. Brown and W. D. M. Rea, Nucl. Data Sheets **120**, 115 (2014).
[50] B. A. Brown, Prog. Part. Nucl. Phys. **47**, 517 (2001).
[51] E. Caurier, M. Rejmund, and H. Grawe, Phys. Rev. C **67**, 054310 (2003).
[52] A. Algora, D. Jordan, J. L. Taín, B. Rubio, J. Agramunt, A. B. Perez-Cerdan, F. Molina, L. Caballero, E. Nácher, A. Krasznahorkay *et al.*, Phys. Rev. Lett. **105**, 202501 (2010).